Influence of the seismic noise characteristics on noise correlations in the Baltic shield

H. A. Pedersen,[1,2,3] F. Krüger[3] and the SVEKALAPKO Seismic Tomography Working Group

[1] *Laboratoire de Geophysique Interne et Tectonophysique, Observatoire de Grenoble, Grenoble University,* BP 53, F-38041 *Grenoble, France.*
E-mail: *Helle.Pedersen@obs.ujf-grenoble.fr*
[2] *GeoForschungsZentrum Potsdam, Germany*
[3] *University of Potsdam, Germany*

SUMMARY

It has recently been shown that correlations of seismic noise can contain significant information about the Green's function along the station profile. Using an array of 38 temporary broad-band stations located in Finland between 1998 September and 1999 March, we study the resulting 703 noise correlations to understand how they are influenced by the directivity of the noise field. The latter information is obtained through f-k analysis of data from two permanent seismic arrays in Germany and Norway and from a subset of stations of the array in Finland. Both types of analysis confirm that the characteristics of the seismic noise is strongly frequency-dependent. At low frequencies (0.02–0.04 Hz), we observe diffuse noise and/or randomly distributed sources. In contrast, the noise is strongly direction-dependent and not fully diffuse in the intermediate period ranges (0.04–0.25 Hz) which correspond to the first and second microseismic peak, created at the Irish and Scottish coast and the western coast of Norway. In this frequency interval the noise is sufficiently close to a plane wave to introduce systematic errors in group velocities for station pairs which are not parallel to the direction of the dominant incident noise. Phase velocities calculated by slant stack over many traces are however correct, independently of profile direction. In the high-frequency band (0.25–1.0 Hz), the situation is a mix between the low-frequency and the intermediate frequency cases. Average phase velocities and individual group velocities from well-oriented profiles are in excellent agreement with results from Rayleigh wave studies of the area.

Key words: seismic noise, surface waves, tomography.

GJI Seismology

1 INTRODUCTION

Techniques using seismic noise for surface wave tomography in California (Sabra *et al.* 2005b; Shapiro *et al.* 2005) open exciting prospects for crustal tomography. Such techniques are based on the assumption that seismic noise is diffuse, and therefore, it is possible to extract a function closely related to the Green's function between two stations by correlating noise recordings from the two sites (Shapiro & Campillo 2004; Sabra *et al.* 2005a). This is possible even when the noise is not perfectly diffuse as long as the noise generators are well distributed. These techniques for determining the (symmetric) elastic Green's function from noise correlations are closely linked to developments in other fields (e.g. Rickett & Claerbout 1999; Weaver & Lobkis 2001; Derode *et al.* 2003), as well as in the analysis of the seismic coda (Campillo & Paul 2003; Malcolm *et al.* 2004; Snieder 2004; Paul *et al.* 2005) which has been shown to be diffuse in its later part (Hennino *et al.* 2001). Seismic records from the Moon are also dominated by a diffuse

wavefield (Larose *et al.* 2005). Campillo (2006) provides a review of the foundation of the method and some possible applications in seismology.

There are still many unresolved issues in relation to such studies, in understanding the nature of the seismic noise and of how to improve the processing techniques. A fundamental issue is how to reconcile the idea of a diffuse wavefield with observations of very distinct areas of oceanic noise generators (e.g. Friedrich *et al.* 1998), as the analysis methods behind such results are based on an assumption of plane-wave propagation.

Surface waves generally have a very complex diffraction. The fundamental mode Rayleigh wave is however relatively simple as it is mainly forward scattered and is only weakly coupled to other surface wave modes (Snieder 1986). This frequency and structure-dependent diffraction will determine at which distances from the noise sources the noise wavefield will become diffuse. To use seismic noise for tomography, we need therefore, to better understand whether noise correlations can be used everywhere, or whether their
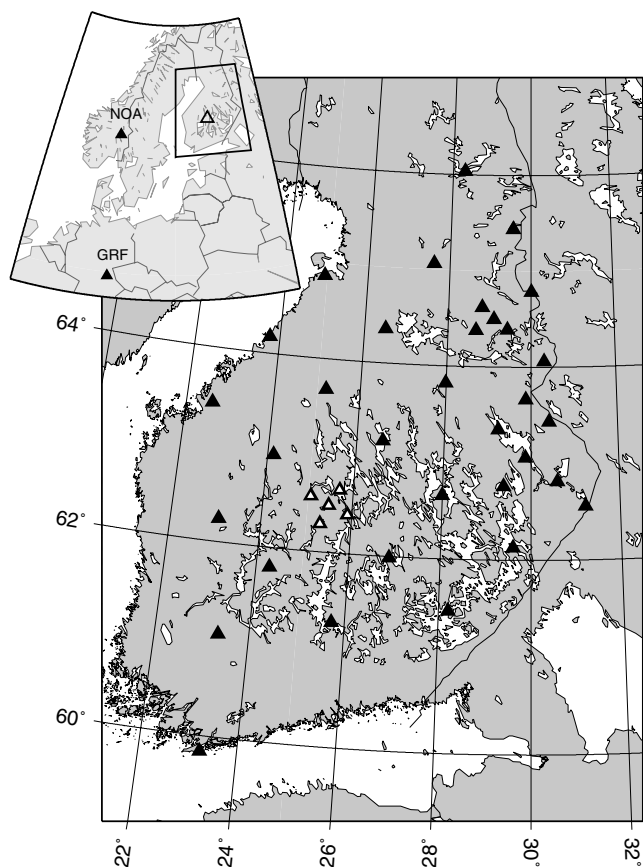
Figure 1. Array geometry. All stations (triangles) have broad-band sensors. The open triangles show the SVEKA subarray. Locations of permanent seismological arrays are marked by black triangles in the inset and the SVEKA subarray is marked by an open triangle.

relevance is dependent on distance to noise generators and/or the scattering characteristics of the Earth's crust.

　The aim of this study is to contribute towards a better understanding of these issues through the analysis of an exceptional data set from the Baltic shield (the SVEKALAPKO passive seismic experiment, Bock & the SSTWG (2001), see Fig. 1) . We have selected this data set as the number of broad-band stations is high (38) within an area where the lateral variations in crustal velocities are small. Even though the Moho depth varies greatly (Sandoval *et al.* 2003), the lower crust in the thickened part is dominated by high velocities and densities (Kozlovskaya *et al.* 2004), so the influence on surface wave phase velocities is small. The homogeneity of the seismic structure on a macroscopic level is confirmed by the small lateral changes in seismic velocities (a few percent) of 15 s period Rayleigh waves (Bruneton *et al.* 2004b), compared to at least 20 per cent in California at the same period (Shapiro *et al.* 2005). Local differences in elastic properties beneath the SVEKALAPKO array, therefore, have little influence on correlation traces derived from the seismic noise. The bedrock installations and the access to electrical current at each site ensured a high recording rate and good quality records. Stehly *et al.* (2006) show that the ocean generated noise varies over the seasons in some frequency bands. Consequently, the main limitation of the data is that they are obtained during the winter season, so that our results are not representative of the noise field over the whole year.

　Prior to the noise correlations, we characterize the coherent wave arrivals within the noise by *f*-*k* analysis of continuous data from

two seismological permanent arrays in Germany and Norway and from a subset of five clustered stations within the SVEKALAPKO array. This technique makes it possible to locate the source areas of the seismic noise for the duration of the experiment.

2 *F*-*K* ANALYSIS OF THE SEISMIC NOISE

Gutenberg showed that primary and secondary ocean microseisms observed throughout Europe are generated in a few dominant regions of the north-eastern Atlantic region (Gutenberg 1912, 1921, 1936). More recent studies update his work for central and northern Europe (Szelwis 1982; Darbyshire 1992; Friedrich *et al.* 1998; Essen *et al.* 1999, 2003). Primary and secondary microseisms are expected to be the dominant contributors to the noise wavefield in certain frequency ranges. Primary microseisms are generated by the interaction between the swell and the sea bottom, and their spectra directly reflect the frequency spectrum of the water waves which are dominated by periods of 12–25 s, depending on the fetch distances of the storms. Secondary microseisms, which are dominated by twice the frequency of water waves, are generated by interfering water wavefield components travelling in opposite directions (Longuet-Higgins 1950; Hasselmann 1963).

　Fig. 2 shows an example of seismic noise at a station located in the centre of the SVEKALAPKO array. To explore the difference in noise characteristics in different frequency intervals, we will refer to four frequency bands, FB1–FB4, which cover the intervals 0.02–0.04, 0.04–0.1, 0.1–0.25 and 0.25–1 Hz. FB2 and FB3 correspond to the intervals with the primary (FB2) and secondary (FB3) microseismic peak.

2.1 Data and processing

Two permanent seismological arrays in the region are adequate for analysing the frequency band of interest, that is, 0.02–1 Hz. The NOA array, of 70 km aperture, in southern Norway has six broadband stations and more than 40 short-period sensors distributed in smaller subarrays of a few kilometres aperture around the broadband stations. The GRF array in southeast Germany has an aperture of about 100 km in the North–South direction and 50 km in the East–West direction, and it is equipped with 13 broad-band stations (see the inset in Fig. 1 for the location of these two arrays). Additionally a subarray of five stations within the SVEKALAPKO array in Finland was used for the array analysis (see the open triangles in Fig. 1, named SVEKA subarray in the following). We use a quasi-continuous frequency-wavenumber technique to analyse the propagation of the noise wavefield during the time span from 1998 September to 1999 March in the frequency bands FB1, FB2 and FB3. For frequency band FB4 the arrays are of limited use due to severe spatial aliasing.

　Typical storms in the area typically last days or weeks. For computational feasibility we analyse 1 hr of GRF and NOA data (00:00–01:00) for each day of the duration of the SVEKALAPKO passive seismic experiment (1998 September–1999 March). For the SVEKA subarray, we use the same time spans as for the correlation analysis. The data are pre-filtered with third order Butterworth filters with corner frequencies defined by the frequency bands FB1–FB4 (see Fig. 2) and are resampled due to computational needs. We subsequently apply a frequency-wavenumber analysis (Kværna & Ringdahl 1986) in sliding time windows each with a length of 20 times the longest period in the frequency band under analysis. The
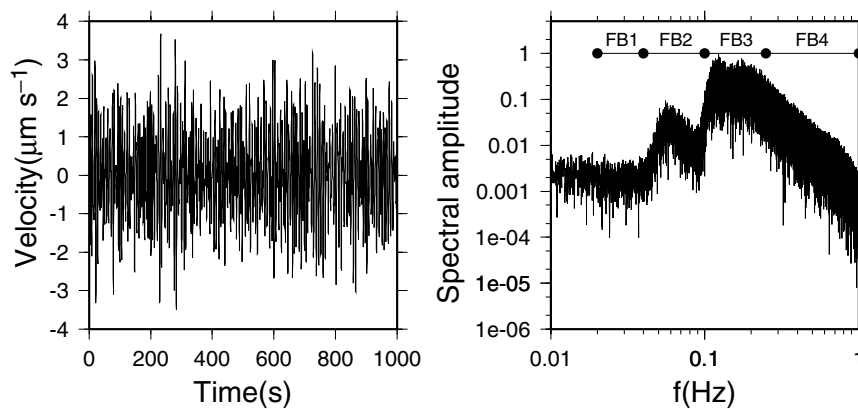
Figure 2. Example of the seismic noise on the vertical component of a randomly chosen station in the centre of the array. Left: traces over a 1000 s long window. Right: normalized spectral amplitudes of 20 000 s noise. The four frequency bands FB1–FB4 are shown by the thin lines. FB2 and FB3 correspond to the frequency intervals with the primary and secondary ocean microseisms.

window lengths are, therefore, 1000 s for FB1 and 80 s for FB4. Two successive windows overlap by 50 per cent. The Cartesian slowness vector domain is finally scanned for beam power and semblance (Neidell & Taner 1971) in a grid from −50 to +50 s per degree with a grid spacing of 1 s per degree.

An inspection of the array transfer functions revealed that all three arrays responses have no severe aliasing for frequency bands FB1 and FB2. For NOA we use only the broad-band stations for these frequency bands. It is not possible to use the SVEKA subarray in FB1 as two out of the five stations are very noisy in this frequency band. The frequency band FB3 starts to be critical in terms of aliasing for all three arrays and it is only due to the width of the frequency band FB3 (10–4 s) that the dominant peak can be identified. The short-period stations of NOA are included in the array analysis for FB3 and FB4 to take advantage of the much smaller interstation distances between the short-period subarray stations. It is possible to use the short-period sensors below their 1-Hz-corner frequency as the secondary ocean microseisms are typically so strong in amplitude that they are the dominant signals after filtering. Frequency band FB4 could not be analysed with GRF and the SVEKA subarray due to severe aliasing.

The maximum semblance was dominated by slowness values of 22–40 s per degree which correspond to surface waves. We therefore, visualize the evolution of the noise with time by averaging the semblance values within the range of the surface wave slownesses and azimuth bins of 10 °, and project the result onto the time axis.

2.2 Result of *f*-*k* analysis

Fig. 3 shows the array results for 1999 January (data gaps are marked by dark grey stripes). The results for the other months are identical except that the overall energy level increases during the autumn, has its peak during winter (1998 December, 1999 January and February) and decreases in 1999 March.

The results for FB1 and FB2/FB3 are significantly different. In FB1 many distinct arrivals with high coherence correspond to surface waves or surface wave coda of teleseismic events (which were not cut out for GRF and NOA, see also caption of Fig. 3). Outside the event windows there is a low coherence background (semblance coefficient about 0.2–0.3) and a wide range of wave azimuths.

In frequency band FB2 all three arrays show clear dominant arrival directions from the West for NOA and subarray SVEKA. Note that SVEKA shows some aliasing projected on easterly azimuths

due to the small number of stations. The NOA array shows small additional arrivals from the North. The GRF array shows a range of directions between West and North with some concentration to the NW. Semblance is also high in FB2 (up to 0.6) for all three arrays but the time spans with high coherence do not correspond to earthquakes. It is likely that the noise has its origin in specific areas off the Norwegian coast to the West and North of NOA. This would explain the Northward azimuths at GRF and the West and North directions at SVEKA and NOA. The Westward directions observed at GRF can be explained by noise generation further West, for example at the Irish and Scottish coast and shelf region which were previously identified as noise generators by Friedrich *et al.* (1998). These noise generators would further enhance the Westward azimuths at SVEKA and NOA.

In frequency band FB3 semblance coefficients are typically smaller than 0.3, that is, less than in FB1 and FB2. There is nevertheless still a dominant propagation from the West, with an additional contribution from northern directions for GRF and NOA. The SVEKA subarray shows stronger aliasing, however a propagation direction from the West can still be identified. As for FB2, the observed directions in FB3 can be explained by noise generation at specific points at the West and North coast and shelf of Norway, with additional energy from more distant locations to the West.

FB4 could only be analysed with NOA, as the spatial aliasing caused deterioration of the results from SVEKA and GRF. The results in FB4 are similar to those of FB3, that is, dominated by waves from the West and to a lesser extent from the North, but the semblance dropped further, to a value of less than 0.1.

Overall the results confirm earlier findings regarding the generation of primary and secondary ocean microseisms in extended but distinct generation areas in northern Europe (Friedrich *et al.* 1998; Essen *et al.* 2003). The decrease in semblance with frequency hints at local and regional causes for the high-frequency scattering. The local scattering is on the contrary low in FB1 as otherwise teleseismic earthquake surface waves would neither be observed clearly nor with high semblance.

3 CORRELATION ANALYSIS

As we have seen in the previous section, the noise field in Finland is particularly coherent (as seen by the high semblance) in frequency band FB2 and less so in the other frequency bands. While the noise is incident from multiple directions in FB1, it is almost uniquely
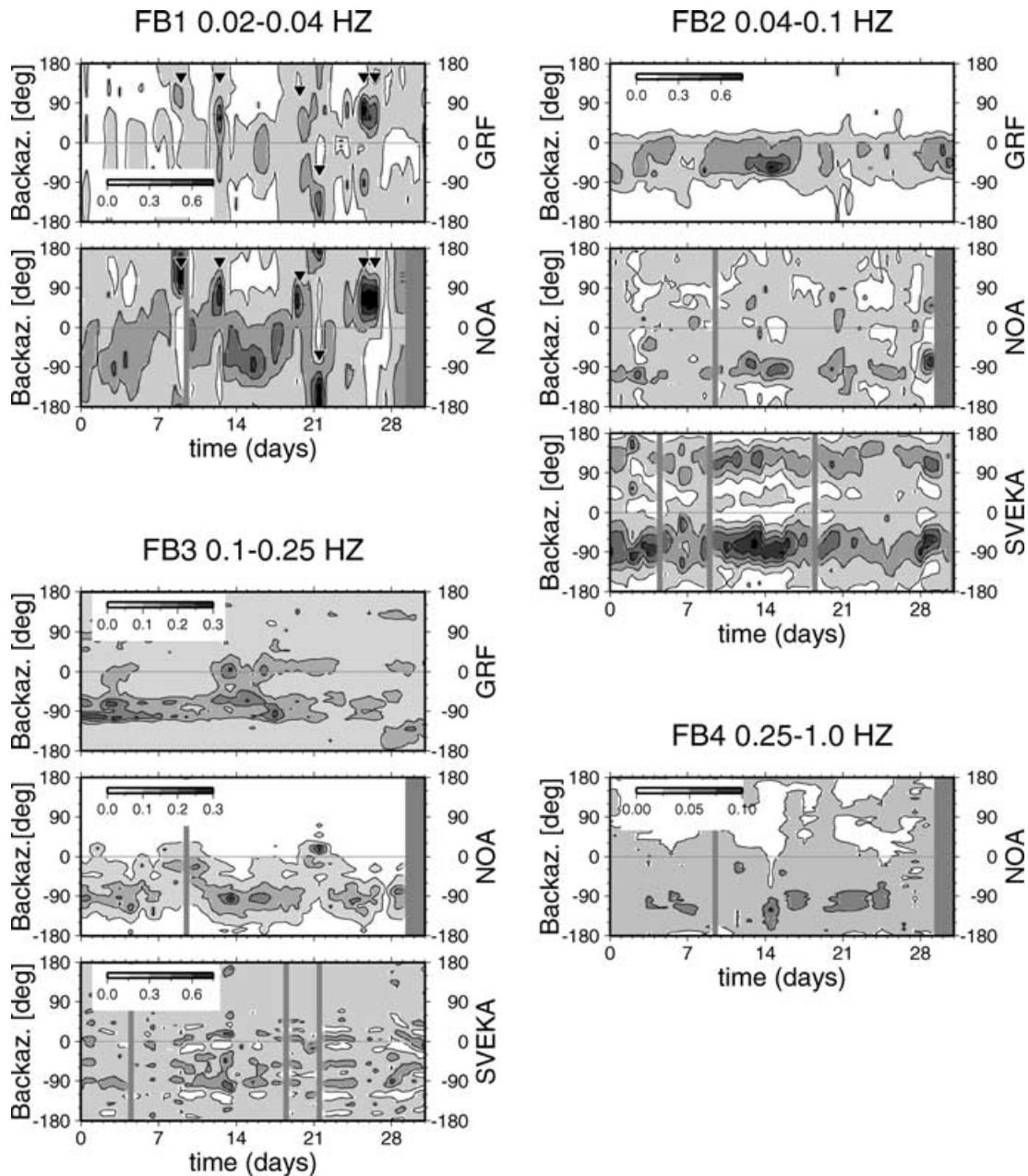
FB1 0.02-0.04 HZ

FB2 0.04-0.1 HZ

FB3 0.1-0.25 HZ

FB4 0.25-1.0 HZ

Figure 3. Results of the array analysis in frequency bands FB1-FB4. Semblance values (grey scale) in the slowness window of surface waves are shown as functions of time for 1999 January for GRF, NOA and SVEKA. The array analysis was not possible for the SVEKA Subarray in FB1 due to poor signal-to-noise ratio. The array analysis for GRF and the SVEKA Subarray could not be used in FB4 due to strong aliasing. Aliasing is also present for SVEKA in FB2 (spurious arrivals from the $90°$ to $120°$) and even more so in FB3, but arrivals from the West ($-90°$) can still be identified. The small areas of high semblance for FB1 (marked by inverted triangles) correspond to earthquakes (NEIC locations: 9-jan-1999 00:07:33.6 14.83N 54.96E $mb = 4.6$; 12-jan-1999 23:22:34.1 0.32S 133.51 E $mb = 5.0$; 19-jan-1999 23:36:13.0 6.95N 123.57E $mb = 4.8$; 21-jan-1999 22:02:16.9 38.65N 142.90E $M_w = 5.8$, here R2 coda; 25-jan-1999 23:45:28.7 2.36N 126.70E $M_w = 5.5$; 26-jan-1999 23:30:36.8 7.69N 126.63E $M_w = 5.2$). Earthquakes do not correspond to high semblance values for frequency bands FB2–FB4.

incident from the West in FB2, and from a wider range of azimuths in FB3 and FB4. In this section, we investigate how these differences influence the correlations of noise recordings from pairs of stations in the area.

3.1 Data and processing

We use data from the 38 broad-band stations for which continuous data are available online (http://www.gfz-potsdam.de/geofon). All

these stations were equipped with either Streckeisen STS2 or Guralp CMG3-ESP 90 s sensors, and the ground velocity was sampled with sampling rates between 20 and 80 Hz. The field experiment lasted approximately 6 months (1998 September–1999 March), with some variability of installation and retrieval date for different stations. As we are focusing on frequencies below 1 Hz, the data were corrected for the instrument response, low-pass filtered and resampled at 2 Hz sampling rate.

The array geometry of the stations is shown in Fig. 1. The array is essentially laid out in a 2-D grid with a regular spacing of

approximately 100 km, even though this pattern in some places is modified by the presence of smaller arrays. The regular grid spacing and the similar elastic properties across the area make it possible to compare correlations for different profiles (different locations and/or profile direction) of almost equal length.

To obtain the Green's function, one must eliminate the influence of earthquakes in the data. There are several ways of doing this. A simple and quick solution is to work on continuous data streams for a period with few or no major earthquakes and disregard the amplitudes completely by using only the sign of the signal (Campillo & Paul 2003; Shapiro & Campillo 2004; Larose *et al.* 2004; Shapiro *et al.* 2005). This approach works because the noise correlations make it possible to extract coherent phase information so that the amplitudes play a minor role. There do however seem to be some limitations with this approach. The principal one is that the frequency bands with low spectral amplitudes will not be adequately represented. This is particularly important when using the extracted signal for tomographic purposes, as the width of the frequency band determines the depth over which one can determine seismic shear velocities. One solution to this shortcoming is to pre-filter the signals around the target frequency prior to correlating them (e.g. Shapiro & Campillo 2004) and carry out the correlations for each target frequency, however it may then be difficult to reconstruct a single broad-band signal. The second problem in applying only the sign function on continuous data is that the influence of seismic events may not be efficiently reduced. For example, a magnitude seven event in our data set gave rise to a peak correlation 10 times higher than that of the noise over the same duration. Such amplitudes may drown in the noise stacks, but the dominance of events to the NE of the SVEKALAPKO array (Japan, Kurile Islands, Aleutian Arc region) may imply that one cannot completely neglect the influence of seismic events.

Overall we consider that there are grounds for exploring other ways of obtaining stable correlations over a large frequency range. Sabra *et al.* (2005a) suggest to apply amplitude clipping when the signal amplitude exceeds some threshold which is determined by the average noise recording for the station in question. This is an intermediate technique between correlating the full signal and the sign of the signal only. We here suggest a processing technique which makes it possible to use the full signal. This correlation procedure focuses mainly on suppressing the influence from earthquakes, explosions and other sources of coherent noise.

We first cut out all seismic events worldwide with magnitudes of five and above. The length of the time window that we reject increases with magnitude, and is 48 hr after a magnitude of seven or above. Secondly, we correlate all remaining overlapping time windows for each pair of stations without pre-filtering to obtain a broad-band correlation function. Of these correlations, we reject those with the highest 10 per cent amplitude (divided by window length) so as to further reduce dominance by small seismic events. This rejection procedure is carried out in the four frequency bands FB1–FB4 (see Fig. 2) where the frequency filtering is done by applying a fifth-order, Butterworth filter in each of the four frequency intervals. The rejection of high-amplitude correlations corresponds to an overall rejection rate of 15–20 per cent of the correlations as some rejected correlations are the same in two or more frequency bands.

For stations operating continuously and simultaneously for the 6 months experiment, the total time duration of the correlations is approximately 5 months, depending on how many of the correlations had high amplitudes in similar frequency bands. The overall time span of stacked correlations was for a few station pairs as low

as 3 months due to differences in installation and retrieval dates, combined with a variable fall out rate for different stations (due to mass centring, disk problems, etc.), but most station pairs have a total length of correlated signals of four to five months.

In the subsequent plots the time axis is oriented so that waves propagating from the eastern half-space into the western half-space arrive at positive times, and the oppositely propagating waves arrive at negative times. With this definition, the positive times for a profile oriented in a given direction ϕ correspond to waves propagating from direction ϕ, while negative times correspond to the opposite direction.

Fig. 4 shows the result of the processing for two different (almost perpendicular) profiles, each of them approximately 300 km long. In the figure, we also show correlations obtained on signals where the amplitude is fully discarded, following the procedure of Campillo & Paul (2003); Shapiro & Campillo (2004); Larose *et al.* (2004); Shapiro *et al.* (2005). We show two examples of such correlations. For one of them, the signals are pre-filtered around the target frequency (i.e. in FB1–FB4) prior to correlation, while for the other one it is not. The spectrum of the recovered correlations is far from flat so we present the results in the four target frequency bands, after filtering with a 5th order zero-phase Butterworth Filter.

Fig. 4 shows that the correlation of the full seismic signals (top trace) does not deteriorate the correlations as compared to the pre-filtered, amplitude-discarded signals (middle trace). It also shows that we obtain a significantly wider band of useable frequencies than if the correlation is applied onto unfiltered, amplitude-discarded signals (bottom trace). It is, therefore, possible to recover a relatively wide frequency band of useable signal by correlating the full signal only once, as long as sufficient care is taken as to rejection of seismic events and other events of high amplitude correlations. The increased number of data manipulations is insignificant as compared to carrying out independent correlations after filtering in each target frequency interval.

3.2 Results of noise correlations: seismic sections

Figs 5 and 6 show the output from the processing in the frequency bands FB1–FB2. The figures for FB3 and FB4 are shown in Appendix A. For each frequency band we show the seismic sections of profiles that are oriented in four directions $\phi \pm 10°$, where ϕ takes the values of 30°, 75°, 120° and 165° clockwise from north. In the remaining part of the paper, and in the figures, we will refer to these directions by N20–N40, N65–N85, N110–N130 and N155–N175.

In this section and those that follow it we use the term 'Noise window' for times smaller than -400 s or bigger than 400 s, that is, where we expect no direct seismic wave arrivals. The term 'Signal Window' (grey shaded in Figs 5 and 6) corresponds to a 100 s wide window around the expected arrival time of the fundamental mode Rayleigh waves (phase velocity approximately 3.3 km s^{-1}). The Signal Window exists for positive and negative times, and overlap at short distances. Finally, the term 'Centre Window' refers to the triangle at small arrival times between the two (negative and positive) Signal Windows.

The behaviour of the seismic traces is very different in the different frequency bands. The signals in FB1 (Fig. 5) are approximately symmetrical and independent of azimuth even though the quality of the signals is highly variable from one trace to another. The amplitude ratio between the waves in the positive and negative Signal Windows typically varies between 0.5 and 2.0, so we are close to the symmetry expected in a fully diffuse wavefield or for a medium
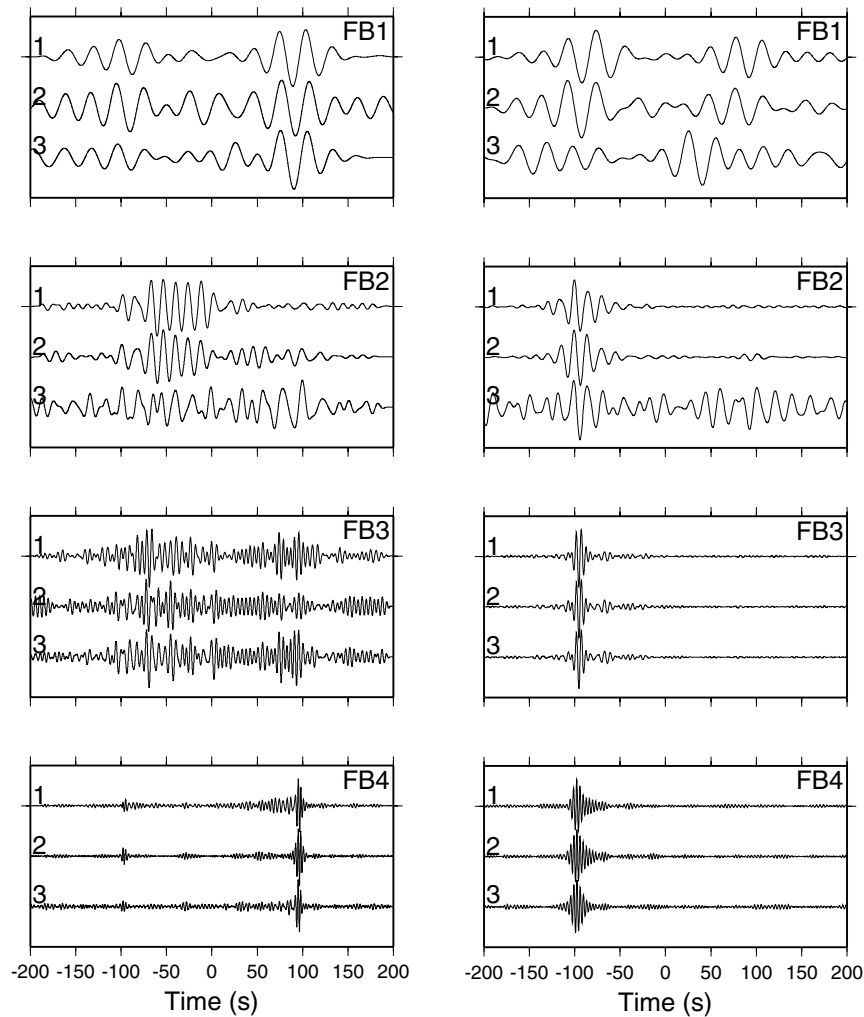
Figure 4. Comparison of the correlation of: (1) full waveform signals (top trace); (2) 1-bit signals (the full waveform multiplied by the sign function, middle trace) after filtering in the target frequency interval and (3) 1 bit signals without pre-filtering (bottom trace). The correlations are subsequently bandpass filtered in the target frequency intervals FB1–FB4. The comparison is shown for two profiles approximately 300 km long and oriented in direction (left) N30 (clockwise angle from the north) and (right) N120. The quality of the correlations is similar between the top (full waveform signals) and centre (amplitude discarded signals after pre-filtering) correlations while the correlation of amplitude discarded signals without pre-filtering have altered waveforms outside the dominant frequencies.

with randomly distributed sources. The wave amplitudes in the two Noise Windows and in the Centre Window are approximately equal and have no apparent variation with azimuth.

The behaviour for FB2 (Fig. 6) is completely different: at N30 and N165 a small coherent wave can be identified within the Signal Window at positive times, however the section is dominated by energy in the Centre Window, mostly at negative times, at N30 and N165. A high-amplitude wave is on the contrary present in the Signal Window at negative times for N75 and N120. The situation is significantly more complex than a simple plane wave from the West: if this were the case, we would observe the projection of the plane wave onto the station profile, that is, coherent energy with an increased apparent velocity $V_{\text{apparent}} = V_{\text{true}}/\cos(\theta)$, where θ is the angle between the slowness vector and the station profile. Another possibility would be that structural changes in the area could cause diffractions that would interfere with the primary waves. The presence of large lateral variations is however in disagreement with tomography results (Bruneton *et al.* 2004b) and also with the fact that traces for profiles of similar length but located in different parts

of Finland are very coherent. Frequency band FB3 is similar to FB2, and frequency band FB4 shows intermediate behaviour to FB1 and FB2 (see Appendix A).

To quantify the amplitude within the Signal Windows and its variation with azimuth over whole seismic sections we calculated the maximum peak envelope of the stack in a 100 s wide window, using velocity reductions between 2.5 and 4 km s^{-1}. A similar calculation was carried out using negative velocities, to obtain the stacked signal amplitude for the opposite direction. We use only traces from station pairs with an interstation distance of more than 200 km for which the Signal Windows at positive and negative times do not overlap. The velocity reduction used was the one that gave the highest envelope amplitude of the stacked traces. The output of this analysis is shown in Fig. 7. For simplicity the actual stacking velocity (varying between 3.1 and 3.7 km s^{-1}, depending on frequency and azimuth) is not annotated, as phase velocities are discussed in more detail in Section 3.3.

Even though the signal amplitude varies with azimuth for FB1, there is significant signal from all directions and the ratio between
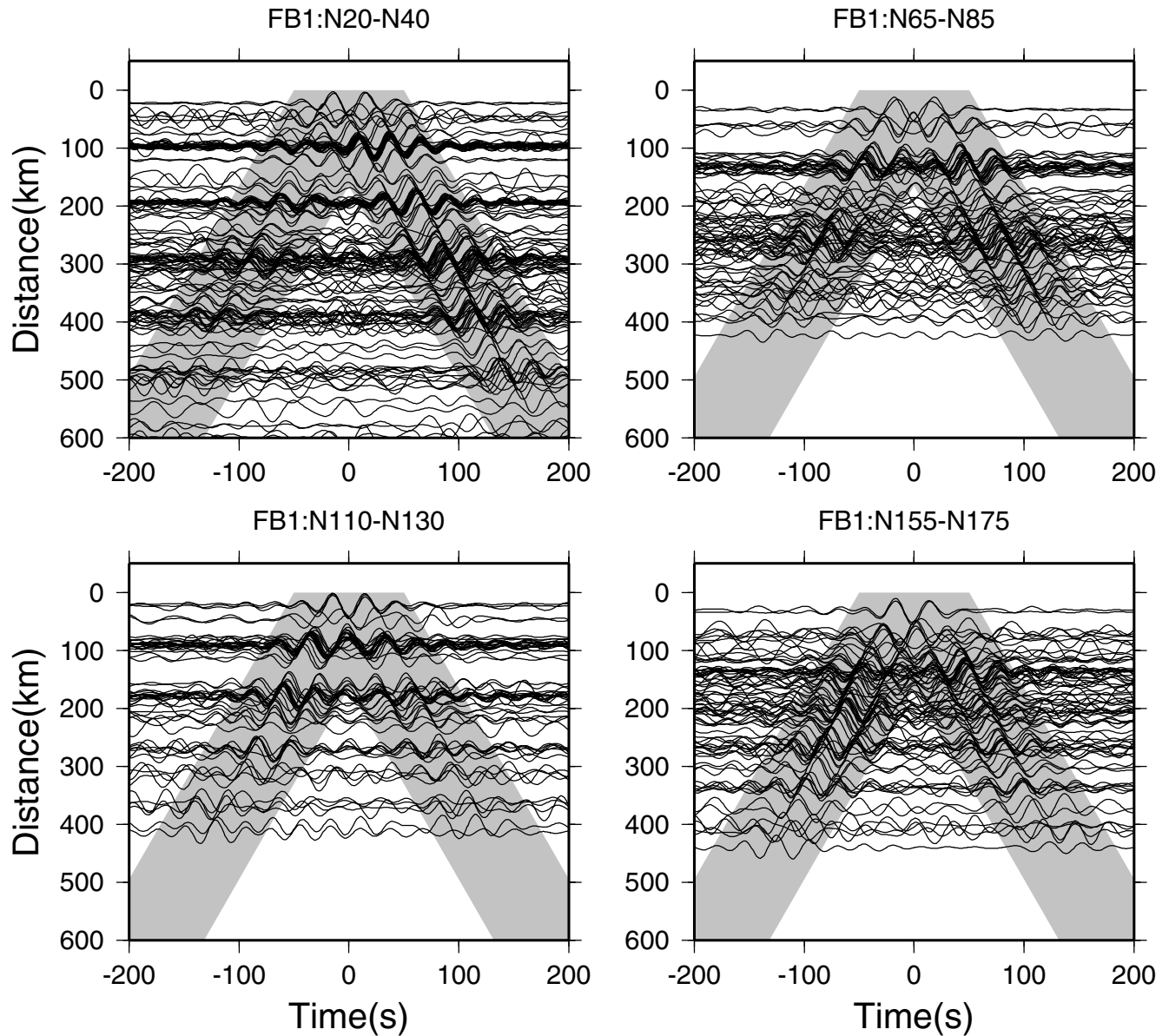
Figure 5. Correlations for four different orientations of station profiles, for frequency band FB1 (0.02–0.04 Hz) obtained by bandpass filtering with a fifth-order zero-phase Butterworth filter. The profile orientations vary by 45° between each plot. The direction of the profiles are give at the top, where Nϕ indicates the (clockwise) angle from the north.

the maximum and minimum signal amplitude is of the order of 8. FB2 has similar behaviour to FB3: the main part of the energy is from W to WNW, and there is almost no energy in approximately three quarters of the azimuths. The amplitude ratio between directions with maximum and minimum stacked amplitudes is approximately 60 for FB2 and 90 for FB3. FB4 has significant energy in approximately a third of the azimuths, and the maximum/minimum amplitude ratio is approximately 40.

If the wavefield is dominated by plane wave fronts incident perpendicular to the profile, the waves would arrive simultaneously at the two stations and the correlation would have its maximum at $t = 0$. This verification corresponds to the analysis of Fig. 7, but without applying a velocity reduction. For FB1, this stack has a variable amplitude as a function of profile direction and has no relationship to the direction of highest signal as observed in Fig. 7. In FB2 the directions of the maximal stack amplitude (when no velocity reduc-

tion is applied) are exactly N and S, that is, perpendicular to the signal stack of Fig. 7, which would point towards plane incident waves. The ratio between maximal and minimal stack amplitudes is however only 6, that is, strongly reduced as compared to the ratio of 60 in Fig. 7. Even if there is some plane wave energy present in FB2 the noise can, therefore, not be composed of purely plane wave fronts from the West. FB3 and FB4 have a mixed behaviour between FB1 and FB2.

3.3 Results of noise correlations: dispersion measurements

With correlations that are influenced by considerable amounts of plane wave energy in FB2 and to a lesser degree in FB3 and FB4, it is necessary to verify whether it is possible to recover reliable phase and group velocities from the noise correlations. Fig. 8 shows the
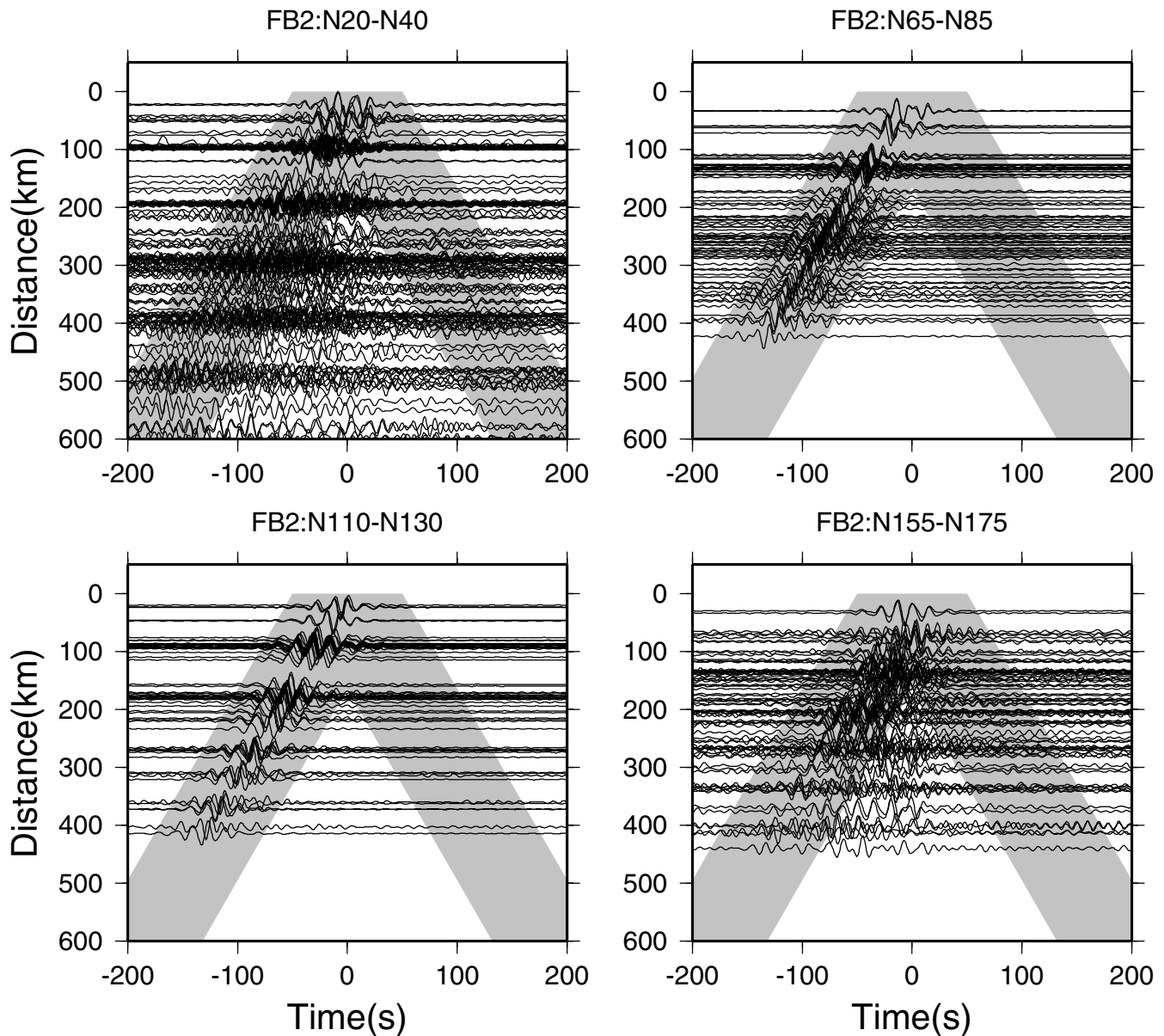
Figure 6. As Fig. 5, for frequency band FB2 (0.04–0.10 Hz).

maximum envelope amplitude of the stacked signals as a function of reduction velocity (slowness) and profile azimuth, for frequency band FB2. This calculation corresponds to the one used for Fig. 7, but this time using a wider range of slownesses. In Fig. 8(a), the overall amplitude is normalized, and consequently the stacked amplitudes from the western directions dominate. When the amplitudes for each azimuth are normalized (Fig. 8b), it becomes clear however that the slowness is constant for the azimuths where it is well defined (i.e. with only one pixel of high amplitudes, N200–N360) and that it does not follow the slowness of a projected plane wave (solid black line). Erroneous slownesses occur only for directions where the highest amplitudes are spread over several slowness pixels (N0–N200).

Even though the recovered phase slowness is stable over the whole array and for a wide range of azimuths the quality of the recovered phase velocity dispersion curve is nevertheless very dependent on the trace selection. Fig. 9 shows an example of the slant stack using all traces in the azimuth range 270°–360° (i.e. profile orientations

90°–180°, stacking with negative reduction velocities). To obtain a good quality dispersion curve at periods over 20 s, we needed to add more traces, that is, use other profile directions. The resulting dispersion curve (not shown here) for periods below 20 s then deteriorated dramatically due to the oscillating phases for profiles not aligned with the noise source in FB2 and FB3. The recovered phase velocities are in very good agreement with the average dispersion curve obtained by the analysis of teleseismic surface waves recorded by the same array (Bruneton *et al.* 2004a). Note that it is in general very difficult to obtain well-constrained phase velocities below 20s period by analysis of teleseismic events, as the unwrapping is difficult in the presence of multipathing and noise when the distance between stations is significantly longer than a wavelength. Noise correlations suffer much less from multipathing at comparable periods due to a much shorter propagation path (profile length 100–800 km) as compared to the earthquake-station distance (typically more than 5000 km in the case of Finland). The small amount
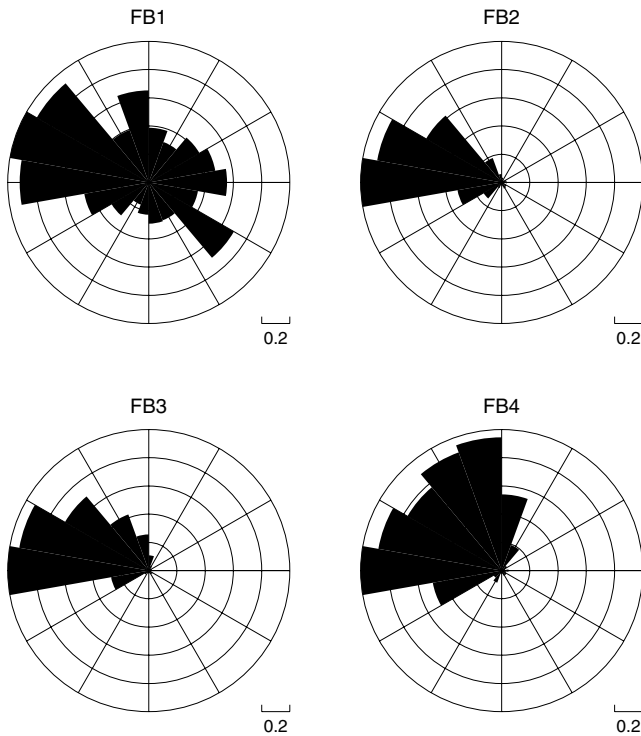
FB1

FB2

0.2

0.2

FB3

FB4

0.2

0.2

Figure 7. Signal amplitude as a function of azimuth in frequency bands FB1 to FB4. The signal amplitude is calculated as the maximum envelope amplitude of the stacked correlations after application of a reduction velocity prior to stack. The reduction velocity is for each azimuth the velocity between 2.5 and 4.0 km s^{-1} which gives the highest stack amplitude. It varies for all directions and frequency bands between 3.1 and 3.7 km s^{-1}.

Figure 9. Phase velocity dispersion curve obtained by slant stack using all traces oriented N270–N360. The grey scale shows the (overall normalized) stack amplitude. The white solid line, which shows the dispersion curve of Bruneton *et al.* (2004a) as obtained by analysis of teleseismic events recorded at the SVEKALAPKO array, is in excellent agreement with the one obtained by analysis of the correlations.

of multipathing is observed by the quasi-absence of coda in the correlations, see Fig. 6). The signal to noise ratio of the correlations at short periods is also much higher than for teleseismic events in well-oriented profile directions. Noise correlations, therefore, provide a semi-automatic way to obtain this high-frequency part of the dispersion curve as long as sufficient precaution is taken in terms of trace selection.

The analysis of group velocities, i.e. analysis of individual traces, is however problematic due to the directionality of the noise field. If the energy propagates as a plane wave, we will observe group slownesses which depends strongly (cosine) on the profile direction. This is indeed what we observe in some cases, as can be seen in Fig. 10. The group slowness was calculated as D/t, where t is the time of the maximum envelope after the bandpass filter (FB1–FB4) and D is the length of the profile. This corresponds to a multiple filter analysis, using only four filters. Frequency band FB1 shows a rather strong scatter around the target slowness of approximately 0.3 s km^{-1}, but the scatter is independent of backazimuth. FB2 does on the contrary show a clear cosine dependence (exemplified by
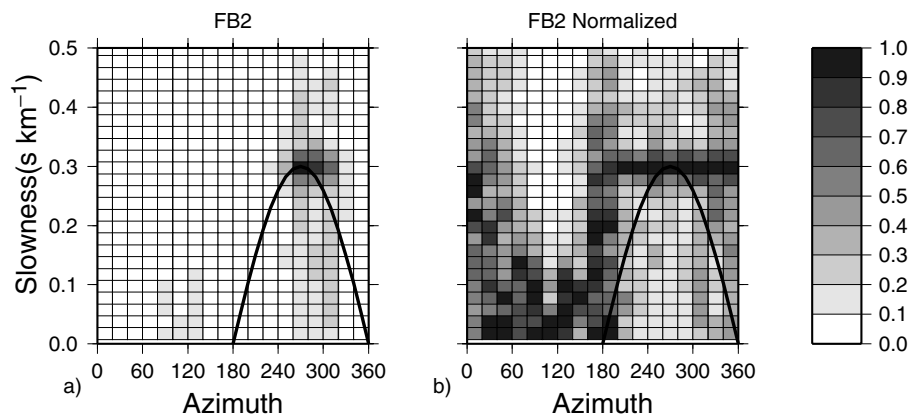
FB2

FB2 Normalized

a)

b)

Figure 8. Evolution of phase velocity with azimuth in frequency band FB2. The plot shows the maximum amplitude of the envelope (grey scale) of the stacked correlations as a function of backazimuth and slowness (the inverse of the reduction velocity applied for the stack). At each azimuth, the phase velocity can be estimated as the inverse of the slowness with the highest stack amplitude. (a) Overall normalization of the amplitudes. In this case the plot is dominated by the westerly directions, and the phase slowness (approximately 0.3 s km^{-1}) can only be identified within a narrow azimuth interval. (b) As (a), but with the amplitudes normalized to unity for each backazimuth window. We see that the phase slowness of 0.3 s km^{-1} is constant over a wide range of azimuths (N200–N360). Outside this azimuth range the choice of 'best' phase slowness is not well defined as high stack amplitudes are present for several slowness pixels. If the correlations were dominated by plane waves incident from the west (270°) the phase slowness would have followed the black cosine curve.
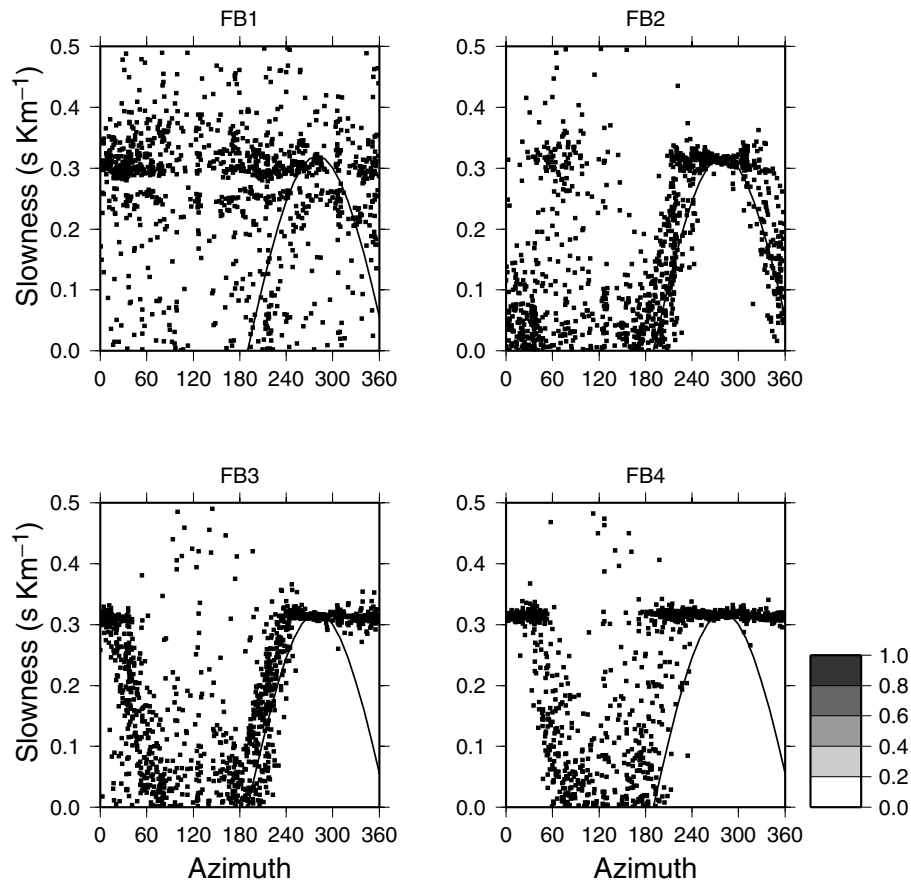
Figure 10. Group slownesses for each of the 703 traces, in the frequency bands FB1 (top left) to FB4 (bottom right). The group slowness is obtained as t/D where t is the time corresponding to the maximum envelope of the filtered trace and D is the profile length. This procedure corresponds closely to applying a multiple filter analysis onto the signals, but with only four frequency filters. The solid line (cosine) corresponds to group slownesses which would be expected the incident energy is that of a plane wave propagating across the array from direction N290.

the black solid line) with the profile direction within the western half-space while the eastern azimuths show a random scatter. This azimuth dependence is independent on the processing method: it was equally strong if the group velocities were calculated for correlations calculated using pre-filtered signals where the amplitudes had been fully discarded. The group velocities for FB2 are consequently reliable only in a narrow azimuth range, between N260 and N280. Outside this range (in the western half-plane), velocity variations are dominated by the projection of the energy front onto the profile, even for traces with a good signal-to-noise ratio (see Fig. 6, direction N65–N85). FB3 and even more so FB4 have a wider range of azimuths where the group slownesses are indicative of the wave velocity, but at each extremity of this stable azimuth interval they follow the shape of a cosine curve rather well.

In spite of the problems with individual group velocities, there is no doubt that the traces in the favourable directions can be used for tomography purposes. Fig. 11 shows the group velocity dispersion curve for a station pair in direction N290 in the northern part of the array. The dispersion curve is calculated by reassigned multiple filter analysis (Kodera *et al.* 1976; Auger & Flandrin 1995; Pedersen *et al.* 2003), and corresponds very well to group velocities observed for a quarry blast along an array of seismic stations in north-eastern Finland (Pedersen & Campillo 1991). The comparison with other E–W profiles shows that group velocities vary up to 3 per cent in the uppermost crust across the area. Due to the rapid group velocity
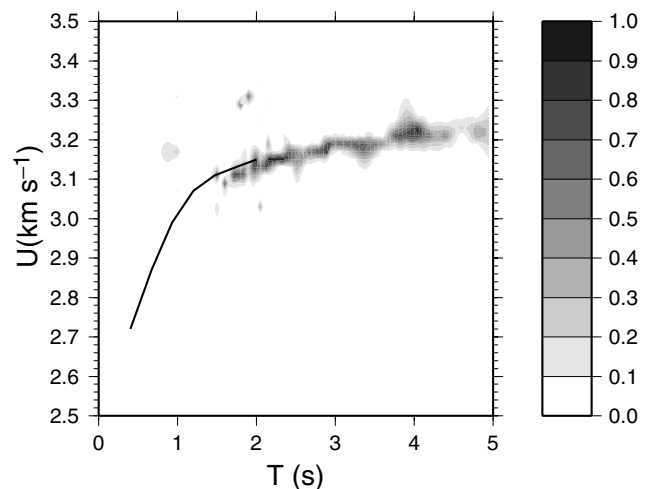

Figure 11. Group velocities for an E–W oriented station profile in northern Finland. The group velocities are obtained by reassigned multiple filter analysis (Kodera *et al.* 1976; Auger & Flandrin 1995; Pedersen *et al.* 2003). The solid line shows group velocities obtained in the same area by Pedersen & Campillo (1991) for records of a quarry blast.

variations with profile direction it is not obvious whether a crustal tomography is possible in an area with so small lateral variations when the noise field is strongly directional.

4 CONCLUSIONS

It is possible to correlate full waveform signals and thereby retrieve a reliable signal over a relatively large frequency band (2–35 s period). Particular care must however be taken to reject seismic events and correlations with a high amplitude. The quality of the retrieved signal is comparable to that obtained using only the sign of the signal after pre-filtering around each target frequency. If one wants to focus only on the longest periods, the use of the sign is possibly slightly better and definitely faster as the sampling rate of the signals can be significantly reduced. To obtain a broad-band signal it was essential to cut out seismic events, and the rejection of the highest amplitude correlations also made it possible to increase the signal quality.

The phase and group velocities obtained using the noise correlations (using favourably oriented profiles) are almost identical to independent measurements in the area of average phase velocities from teleseismic waves (Bruneton *et al.* 2004a) and of group velocities in northern Finland from a quarry blast (Pedersen & Campillo 1991). This confirms that the retrieved waves of vertical-component correlations are fundamental mode Rayleigh waves (e.g. Shapiro & Campillo 2004). No other waves could be identified in the group or phase velocity plots.

Our analysis shows that the noise field in the study area is dominated during wintertime by waves from the western half-space at short periods ($T < 20$ s). The direction corresponds well to a domination of ocean-generated noise, possibly along the West coast of southern Norway (and the northern coast at short periods) and/or by previously identified noise generators West of Ireland and North of Norway.

Obtaining the Green's function depends on either a fully diffuse wavefield or well-distributed noise sources. The noise field that we observe does not fulfil these criteria in all frequency bands. In particular, the ocean generated noise is a complex mix of diffuse and subplane wave energy: it is sufficiently diffuse so that coherent phases over all station pairs correspond well to fundamental mode Rayleigh waves, but sufficiently close to plane waves so that the group velocities at individual stations are strongly dependent on the direction of the station profile. One can represent such wavefields as a composition of subplane energy fronts, each of which having strong phase perturbations.

These conclusions may well be strongly dependent on the distance to the noise generators, so that they may not be applicable to all areas of the world. They may also well be season dependent, but we do not have data from the area to carry out a similar analysis over the summer months. It is nevertheless clear that even though noise correlations are a promising tool for the investigation of the Earth's crust, caution must be taken as to the nature of the noise field, implying careful selection of station profiles for which the group velocities are used for tomography. Interestingly the characteristics of the deterministic part of the noise field were similar in Norway (NORSAR), Germany (Gräfenberg Array GRF) and Finland (five-station subarray SVEKA in the centre of Finland). One possibility for a safe use of noise correlations would be to determine the noise directionality with dedicated small dense array(s) in the study area. The main advantage compared to analysing teleseismic events is the easy extension of the dispersion curve to higher frequencies, to give further constraints on the crustal structure.

REFERENCES

Auger, F. & Flandrin, P., 1995. Improving the Readability of Time-Frequency Time-scale Representation by the Reassignment Method, *IEEE Transactions on Signal Processing,* **43**(5), 1068–1089.

Bock, G. & the SVEKALAPKO Seismic Tomography Working Group (SSTWG), 2001. Seismic Probing of the Fennoscandian Lithosphere, *EOS, Trans. Am. geophys. Un.,* **82,** 621, 628–629.

Bruneton, M., Pedersen, H.A., Vacher, P., Kukkonen, I.T., Arndt, N.T., Funke, S., Friederich, W., Farra, V. & the SVEKALAPKO Seismic Tomography Working Group, 2004a. Layered lithospheric mantle in the central Baltic Shield from surface waves and xenolith analysis, *Earth planet. Res. Lett.,* **226,** 41–52.

Bruneton, M., Pedersen, H.A., Farra, V., Arndt, N.T., Vacher, P. & the SVEKALAPKO Seismic Tomography Working Group, 2004b. Complex lithospheric structure under the central Baltic Shield from surface wave tomography, *J. geophys. Res.,* **109,** B10303.

Campillo, M., 2006. Phase and correlation in 'Random' seismic fields and the reconstruction of the Green Function, *Pure appl. Geophys.,* **163,** 475–502.

Campillo, M. & Paul, A., 2003. Long range correlations in the seismic coda, *Science,* **299,** 547–549.

Darbyshire, J., 1992. Microseisms formed off the coast of Norway, *Phys. Earth planet. Inter.,* **73,** 282–289.

Derode, A., Larose, E., Tanter, M., de Rosny, J., Tourin, A., Campillo, M. & Fink, M., 2003. Recovering the Green's function from field-field correlations in an open scattering medium, *J. acoust. Soc. of Am.,* **113,** 2973–2976.

Derode, A., Larose, E., Campillo, M. & Fink, M., 2003. How to estimate the Green's function of a heterogeneous medium between two passive sensors? Application to acoustic waves, *Appl. Phys. Lett.,* **83**(15), 3054–3056.

Essen, H.-H., Klußmann, J., Herber, R. & Grevemeyer, I., 1999. Does microseisms in Hamburg (Germany) reflect the wave climate in the North Atlantic? *Deutsche Hydrographische Zeitschrift,* **51,** 33–45.

Essen, H.-H., Krüger, F., Dahm, T. & Grevemeyer, I., 2003. On the generation of secondary microseisms observed in northern and central Europe, *J. geophys. Res.,* **108**(B10), 2506, doi:10.1029/2002JB002338.

Friedrich, A., Krüger, F. & Klinge, K., 1998. Ocean-generated microseismic noise located with the Grnberg array, *J. Seism.,* **2,** 47–64.

Goldstein, P., Dodge, D. & Firpo, M., 1999. SAC2000: Signal processing and analysis tools for seismologists and engineers, in *IASPEI International Handbook of Earthquake and Engineering Seismology, Part B, Int. Geophys. Ser.,* Vol. 81, pp. 1613–1614, eds Lee, W., Kanamori, H., Jennings, P. & Kisslinger, C., Academic, San Diego, California.

Gutenberg, B., 1912. Die seismische Bodenunruhe, *Betr. Z. Geophysik,* **11,** 314–353, *in German*.

Gutenberg, B., 1921. Untersuchungen über die Bodenunruhe mit Perioden von 4 s–10 s in Europa, *Veröff. d. Zentralbureaus der int. Seism. Assoc.,* p. 106, *in German*.

Gutenberg, B., 1936. On microseisms, *Bull. seism. Soc. Am.,* **26,** 111–117.

Hasselmann, K., 1963. A statistical analysis of the generation of microseisms, *Rev. Geophys.,* **1,** 177–210.

Hennino, R., Tr'gour's, N., Shapiro, N., Margerin, L., Campillo, M., van Tiggelen, B. & Weaver, R.L., 2001. Observation of Equipartition of seismic waves in Mexico, *Phys. Rev. Lett.,* **86**(15), 3447–3450.

Kodera, K., de Velledary, C. & Gendrin, R., 1976. A new method for the numerical analysis of non-stationary signals, *Phys. Earth. planet. Int.,* **12,** 142–150.

Kozlovskaya, E., Elo, S., Hjelt, S.-E., Yliniemi, J., Pirttijrvi, M. & SVEKALAPKO STWG, 2004. 3D density model of the crust of southern and central Finland obtained from joint interpretation of SVEKALAPKO crustal P-wave velocity model and gravity data, *Geophys. J. Int.,* **158,** 827–848.

Kværna, T. & Ringdahl, F., 1986. Stability of various f-k estimation techniques, in *Semiannual Technical Summary, 1 Oct. 1985–31 March 1986, NORSAR Scientific Report, 1-86/87, Kjeller*, *Norway*, pp. 29–40.

Larose, E., Derode, A., Campillo, M. & Fink, M., 2004. Imaging from one-bit correlations of wide-band diffuse wave-fields *J. Appl. Phys.,* **95**(12), 8393–8399.

Larose, E., Khan, A., Nakamura, Y. & Campillo, M., 2005. Lunar Subsurface Investigated from Correlation of Seismic Noise, *Geophys. Res. Lett.,* **32,** L16201, doi:10.1029/2005GL023518.

Longuet-Higgins, M.S., 1950. A theory of the origin of microseisms, *Phil. Trans. R. Soc. Lond.,* A, **243,** 1–35.

Malcolm, A.E., Scales, J.A. & van Tiggelen, B.A., 2004. Extracting the Green function from diffuse, equipartitioned waves, *Phys. Rev. E,* **70,** 015 601, doi:10.1103/PhysRevE,70,015601.

Neidell, N.S. & Taner, T., 1971. Semblance and other coherency measures for multichannel data, *Geophysics,* **36,** 482–497.

Paul, A., Campillo, M., Margerin, L., Larose, E. & Derode, A., 2005. Empirical synthesis of time-asymmetrical Green functions from the correlation of coda waves, *J. geophys. Res.,* **110,** B08302, doi:10.1029/2004JB003521.

Pedersen, H.A. & Campillo, M., 1991. Depth dependence of Q beneath the Baltic Shield inferred from modelling of short period seismograms, *Geophys. Res. Lett.,* **18,** 1755–1758.

Pedersen, H.A., Mars, J. & Amblard, P.-O., 2003. Improving group velocity measurements by energy reassignment, *Geophysics,* **68,** 677–684.

Rickett, J. & Claerbout, J., 1999. Acoustic daylight imaging via spectral factorization: helioseismology and resevoir monitoring, *Leading Edge,* **18,** 957–960.

Sabra, K.G., Gerstoft, P., Roux, P., Kuperman, W.A. & Fehler, M.C., 2005a. Extracting time-domain Green's function estimates from ambient seismic noise, *Geophys. Res. Lett.,* **32,** L03310, doi:10.1029/2004GL021862.

Sabra, K.G., Gerstoft, P., Roux, P., Kuperman, W.A. & Fehler, M.C., 2005b. Surface wave tomography from microseisms in Southern California, *Geophys. Res. Lett.,* **32,** L14311, doi:10.1029/2005GL023155.

Sandoval, S., Kissling, E., Ansorge, J. & the SVEKALAPKO STWG, 2003. High-resolution body wave tomography beneath the SVEKALAPKO array: I. A-priori 3D crustal model and associated traveltime effects on teleseismic wavefronts, *Geophys. J. Int.,* **153,** 75–87.

Shapiro, N.M. & Campillo, M., 2004. Emergence of broadband Rayleigh waves from correlations of the ambient seismic noise, *Geophys. Res. Lett.,* **31,** L07614, doi:10.1029/2004GL019491.

Shapiro, N.M., Campillo, M., Stehly, L. & Ritzwoller, M., 2005. High resolution surface wave tomography from ambient seismic noise, *Science,* **307,** 1615–1618.

Snieder, R., 1986. 3D linearized scattering of surface waves and a formalism for surface wave holography, *Geophys. J. R. astron. Soc.,* **84,** 581–605.

Snieder, R., 2004. Extracting the Green's function from the correlation of coda waves: a derivation based on stationary phase, *Phys. Rev. E,* **69,** doi:10.1103/PhysRevE.69.046610.

Stammler, K., 1993. Seismichandler—programmable multichannel data handler for interactive and automatic processing of seismological analyses, *Comput. Geosci.,* **19**(2), 135–140.

Stehly, L., Campillo, M. & Shapiro, N.M., 2006. A study of the seismic noise from its long range correlation properties, *J. geophys. Res.,* in press.

Szelwis, R., 1982. Modeling of microseismic surface wave sources, *J. geophys. Res.,* **87,** 6906–6918.

Weaver, R.L. & Lobkis, O.I., 2001. Ultrasonics without a source: thermal fluctuation correlations at MHz frequencies, *Phys. Rev. Lett.,* **87,** 134 301, doi:10.1103/PhysRevLett.87.134301.

Wessel, P. & Smith, W.H.F., 1998. New, improved version of Generic Mapping Tools released, *EOS Trans. Am. geophys. Un.,* **79**(47), p. 579.
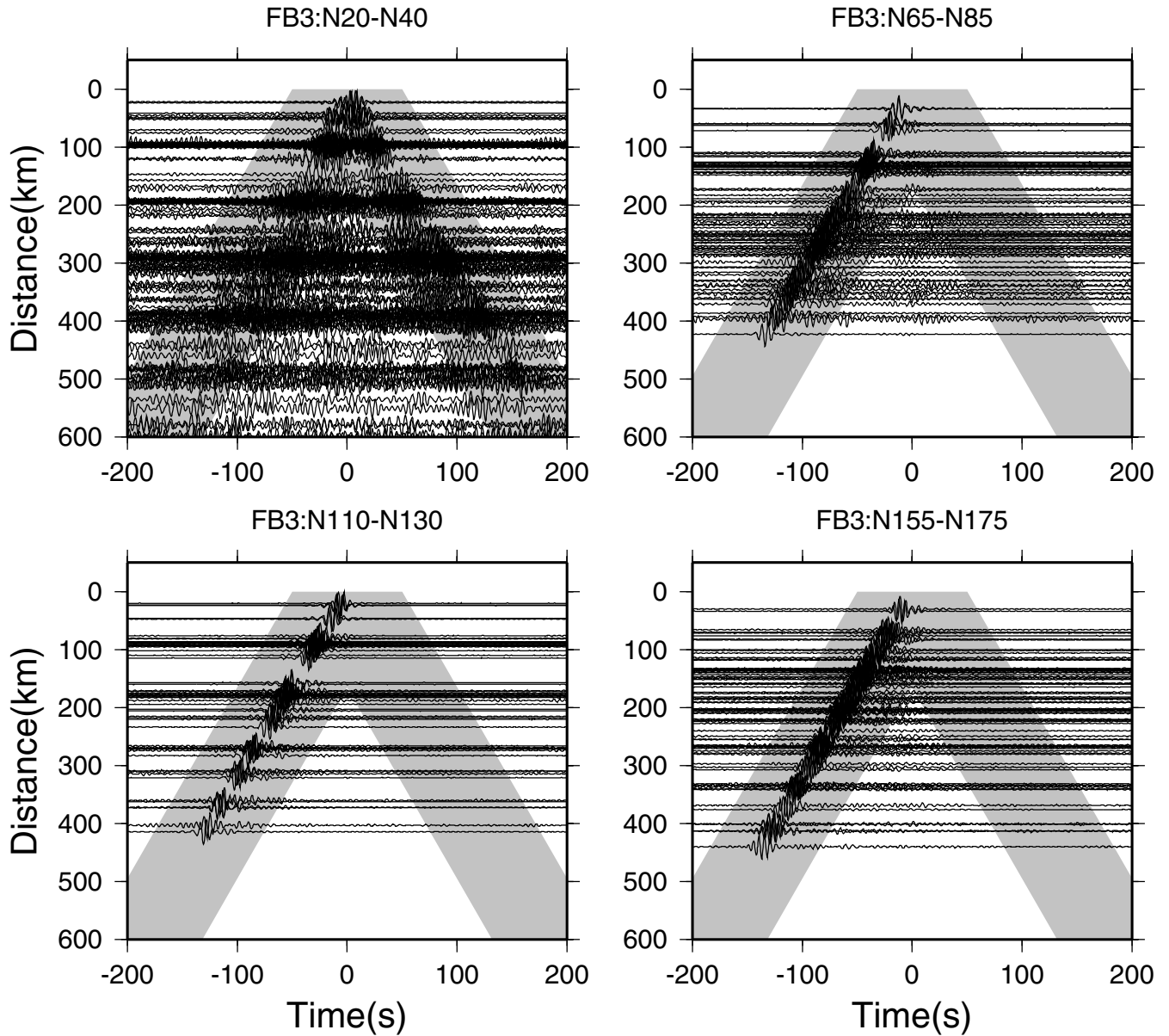
APPENDIX A:

Figure A1. Correlations for four different orientations of station profiles, for frequency band FB3 (0.1–0.25 Hz) obtained by bandpass filtering with a fifth-order zero-phase Butterworth filter. The profile orientations vary by 45° between each plot. The direction of the profiles are give at the top, where Nϕ indicates the (clockwise) angle from the north.
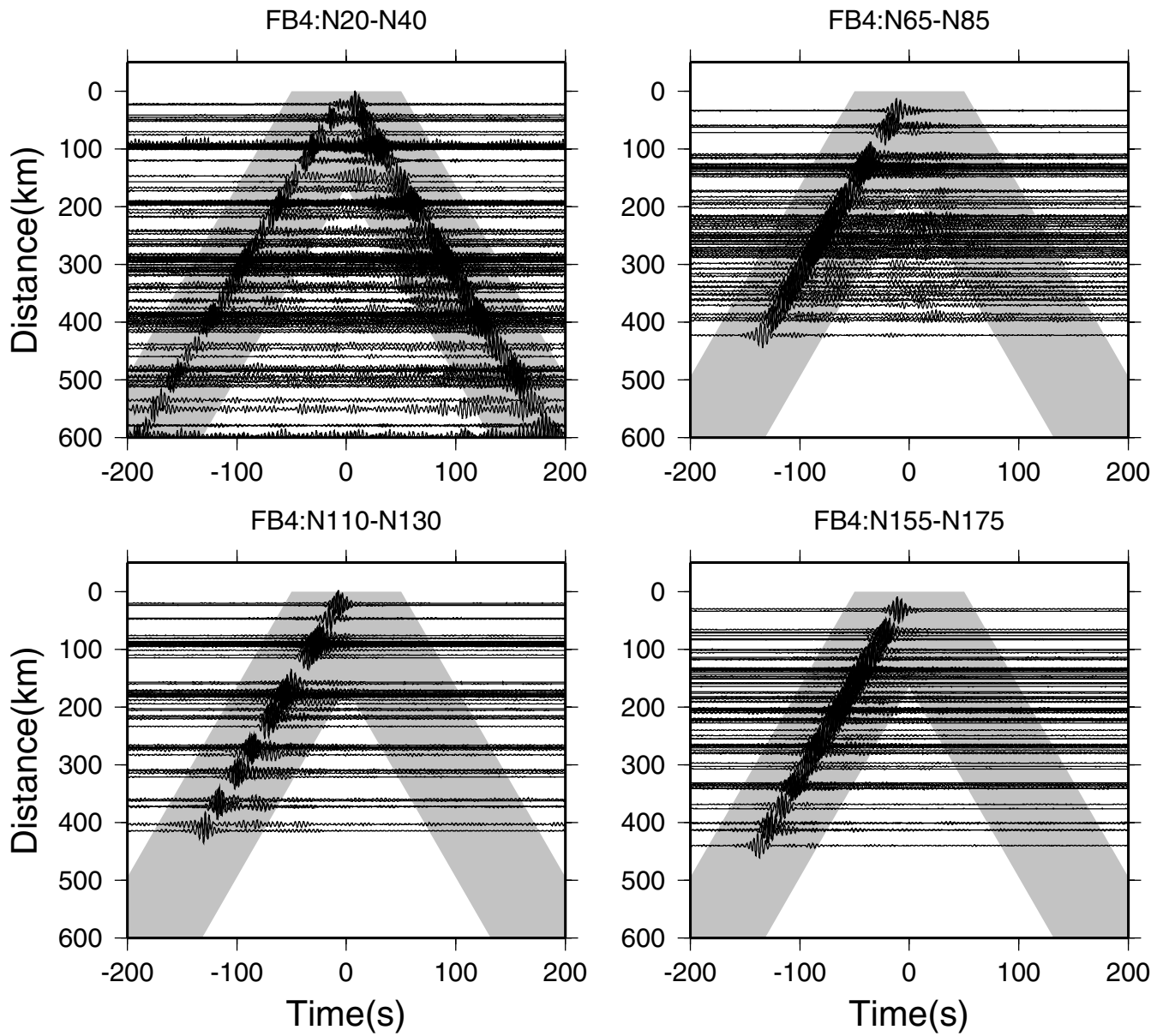
Figure A2. As Fig. A1, for frequency band FB4 (0.25–1.00 Hz).